Eur. Phys. J. B **73**, 471–482 (2010)
DOI: 10.1140/epjb/e2010-00035-4

THE EUROPEAN PHYSICAL JOURNAL B

Regular Article

Tunneling spectroscopy of layered superconductors: intercalated $Li_{0.48}(C_4H_8O)_xHfNCl$ and De-intercalated $HfNCl_{0.7}$

T. Takasaki[1], T. Ekino[2,a], A. Sugimoto[2], K. Shohara[2], S. Yamanaka[3], and A.M. Gabovich[4]

[1] Hiroshima University, Graduate school of Advanced Sciences of Matter, 739-8530 Higashi-Hiroshima, Japan
[2] Hiroshima University, Graduate school of Integrated Arts and Sciences, 739-8521 Higashi-Hiroshima, Japan
[3] Hiroshima University, Graduate school of Engineering, 739-8527 Higashi-Hiroshima, Japan
[4] Institute of Physics of the National Academy of Sciences, Nauka Avenue 46, 03680 Kiev, Ukraine

Received 4 July 2009 / Received in final form 17 November 2009
Published online 27 January 2010 –

Abstract. Tunneling measurements have been carried out on layered superconductors of the β(SmSI)-type – $Li_{0.48}(THF)_xHfNCl$ (THF = C_4H_8O) and $HfNCl_{0.7}$ – by means of break-junction and scanning tunneling spectroscopy. Break-junction technique reveals Bardeen-Cooper-Schrieffer (BCS) – like gap structures with typical gap values of $2\Delta(4.2\ \mathrm{K}) = 11-12$ meV for $Li_{0.48}(THF)_xHfNCl$ with the highest $T_c = 25.5$ K. Some of our measurements revealed multiple gaps and dip-hump structures, the largest gap 2Δ (4.2 K) $\approx$ 17–20 meV closing at T_c. This was shown both by break-junction and scanning-tunneling spectroscopy. From these experiments it stems that the highest obtained gap ratio $2\Delta/k_BT_c \sim 8$ substantially exceeds the BCS weak-coupling limiting values: $\approx$3.5 and $\approx$4.3 for s-wave and d-wave order parameter symmetry, respectively. Such large $2\Delta/k_BT_c$ ratios are rather unusual for conventional superconductors but quite common to high-T_c cuprates, as well as to organic superconductors. Our studies allowed to collect much more evidence concerning the huge pairing energy in those materials and to investigate in detail the complexity of their superconducting gap spectra. An origin of the observed phenomena still remains to be clarified.

1 Introduction

Recently, several kinds of novel superconductors have been found, including MgB_2 [1,2], sesquicarbide [3], and iron-based oxypnictide or pnictide compounds [4–9], which exhibit significantly higher critical temperatures, T_c, than those of any conventional intermetallic superconductors [10,11]. Some of those new compounds possess layered crystal structures containing metal and metalloid ions. The reduced dimensionality is often believed to be substantial for high-T_c superconductivity itself [12,13]. At the same time, the *microscopic* origin of the Cooper pairing in cuprates and the novel compounds is still not known, although many sophisticated theories do exist (see, e.g., Refs. [2,7–9,12,14–19]). Therefore, empiric and semi-phenomenological considerations constitute the main guiding line in the search for new superconductors.

In particular, for MgB_2, a number of experimental reports suggest that strong electron-phonon interactions through oscillations of light-mass B atoms on the honeycomb layer are responsible to realize the high T_c [20,21]. As for oxypnictides, a two-gap electron-hole model with interband Hubbard interaction might be important for realizing high T_c [22].

$Li_{0.48}(THF)_xHfNCl$ (THF (tetrahydrofuran); C_4H_8O) with SmSI-type layered M (Metal)-nitrogen (MN) structure is a high-T_c superconductor found by Yamanaka et al. [23] (see also a review [24]). Superconductivity in this compound is induced by electron doping to HfN double-honeycomb layers through the intercalation of Li ions and organic molecules between Cl layers, which leads to the high $T_c = 25.5$ K. Band calculations showed that strongly hybridized Hf 5d and N 2p orbitals form the conduction band [25,27]. Experimental studies of nuclear magnetic resonance (NMR) [28], muon-spin rotation (μSR) [29] and X-ray absorption [30] are consistent with those predictions. On the other hand, there is another way of electron doping of HfN layers, namely, de-intercalating Cl atoms from β-HfNCl [31]. The resultant material $HfNCl_{1-x}$ exhibits superconductivity with $T_c = 23.5$ K. Upper critical field, H_{c2}, measurements in the related layered superconductor β-$ZrNCl_{0.7}$ with a somewhat lower $T_c \approx 13$ K revealed large H_{c2} anisotropy with respect to an angle between H_{c2} and the double ZrN layer [32]. Finally, specific-heat measurements of the superconducting sample $Li_{0.12}ZrNCl$ with $T_c \approx 12.7$ K showed that the ratio between the superconducting gap $\Delta(0)$ at zero temperature, T, and T_c takes strong-coupling values $2\Delta(0)/k_BT_c \approx 5$ [33]. Here k_B is the Boltzmann constant.

[a] e-mail: ekino@hiroshima-u.ac.jp

In our previous break-junction studies on $ZrNCl_{0.7}$ [34], two kinds of energy gaps, $2\Delta = 8-10$ meV and 3–5 meV, have been observed. The former values correspond to very large gap ratios $2\Delta/k_BT_c = 6.6-8.3$, while the scatter of the latter means $2\Delta/k_BT_c = 2.7-3.8$, which includes the BCS weak-coupling ratio $2\pi/\gamma \approx 3.52$. Here $\gamma = 1.78\ldots$ is the Euler constant. Such large gap magnitudes and multiple gap structures are very rare for conventional superconductors [35]. On the other hand, the ratios $2\Delta/k_BT_c > 6$ are routinely observed in high-T_c cuprates [36] or organic superconductors [37].

Some other features of the nitride compounds, such as low carrier density, the semiconductor-metal transition on carrier doping, the quasi-two-dimensional layered crystal structure, etc. [28] are also similar to those of the copper-based oxides [38–41]. It is remarkable that recent experimental studies of $Li_{0.48}(THF)_xHfNCl$ and $ZrNCl_{0.7}$ revealed a negligibly small isotope effect $T_c \sim M^{-0.07}$ (M is the nitrogen atomic mass) [42,43]. At the same time, the analysis of high-pressure X-ray and Raman scattering results for $Li_{0.5}(THF)_xHfNCl$ and $ZrNCl_{0.7}$ crystals on the basis of the *approximate* strong-coupling McMillan formula [44] led to a large coupling constant $\lambda > 3$ [45]. Thus, to reconcile experimental data of references [42,43] and [45], it seems plausible to invoke a non-phonon superconductivity mechanism.

In this paper, we widened the scope of measurements. In particular, superconducting energy gaps of both β-$Li_{0.48}(THF)_xHfNCl$ and β-$HfNCl_{0.7}$ were found directly from in-situ break junction tunneling spectroscopy. Complementary studies were made as well using scanning tunneling spectroscopy (STS). Some speculations about the nature of superconductivity in the materials concerned are presented on the basis of our and previously published data.

2 Experimental technique and the way of data handling

We have used polycrystalline pellets of Li and THF intercalated superconducting samples $Li_{0.48}(THF)_xHfNCl$ and Cl de-intercalated $HfNCl_{0.7}$. Details of the sample preparation have already been reported [23,24,31]. It should be noted that c-axes of pressed pellets are oriented perpendicularly to the HfN plane of the layered $HfNCl_{0.7}$ [28]. Since the samples are very reactive in a humid air, the preparation was carried out in a pure Ar filled glove box. The tunneling measurements were done using an in-situ break-junction technique [46]. In this method, a sample is cracked at 4.2 K to form a superconductor – insulator – superconductor (SIS) junction with a fresh and unaffected interface, which is obtained by applying the bending force parallel to the thickness (c-axis) direction of the c-axis oriented thin (∼0.3–0.5 mm) pellet. We believe this is the most effective way to fabricate tunnel junctions of this kind from a chemically reactive compound [46–49].

For an SIS junction, the characteristic peak-to-peak bias separation V_{p-p} in the tunneling conductance, $G(V) \equiv dI/dV$, corresponds to $4\Delta/e$, where 2Δ represents the superconducting energy gap between electron-like and hole-like quasiparticles, I is the quasiparticle current, V is voltage, and e is the elementary charge. Such an SIS junction is very sensitive to probe gap edge structures even at high temperature close to T_c because of the convolution between electron gapped densities of states $N_{1,2}(E)$ for both electrodes in the integrand of the equation for $G(V)$ [35,50]; thereby precise measurements are possible even in the vicinity of T_c. We also employed STS measurements with PtIr tip in the ultra high vacuum ($<10^{-8}$ Pa), in order that $G(V)$ measurements in a superconductor – vacuum insulator – normal metal (SIN) junction configuration would provide us with complementary information. This measurement probed the c-plane consisting of the double honeycomb HfN layers, after peeling off the topmost dirty thin layers in UHV LT conditions. In particular, a combination of break-junction and STS experiments allows one to unequivocally distinguish between realizations of SIS or SIN configurations.

To carry out a quantitative analysis, we compare the experimental data with the standard expression for the tunneling conductance across an SIS junction [35]

$$G(V) = \frac{dI(V)}{dV} = C\int_{-\infty}^{+\infty} N_1(E)\frac{dN_2(E+eV)}{dV} \times [f(E) - f(E+eV)] + N_1(E)N_2(E+eV) \times \left[-\frac{df(E+eV)}{dV}\right] dE. \quad (1)$$

Here C and $f(E)$ are the scaling parameter and the Fermi distribution function, respectively. Hereafter, to fit the results we use the complex density-of-states function $N(E, \Gamma)$, which contains a phenomenological broadening parameter Γ that has been originally introduced by Dynes et al. [51] as the lifetime quasiparticle broadening:

$$N(E,\Gamma) = \left|\mathrm{Re}\frac{E - i\Gamma}{\sqrt{(E-i\Gamma)^2 - \Delta^2}}\right|. \quad (2)$$

Here Δ, Γ, and C are fitting parameters.

Taking C in equation (1) as a constant (normal state conductance) is an approximation valid for calculations of currents at small bias voltages, which are relevant for tunneling between superconductors, where a proper energy scale is Δ. This approximation corresponds to energy-independent tunnel matrix elements T_{12}. Harrison showed [52] that in the quasiclassical scheme T_{12} is a product of the reciprocals to the normal-metal quasiparticle densities of states on the left and on the right of the barrier times the tunnel integral. Therefore, those densities of states cancel out from the net expressions for the tunneling rate (see also Refs. [35,53–55]. On the contrary, the gap-induced square-root factors in the superconducting quasiparticle densities of states appear explicitly [56] in expressions for tunnel currents and conductivities in a way similar to our equation (2). The same kind of approximation is used for Josephson currents between conventional superconductors [57,58].

Formula (2) describes the lifetime broadening, which always takes place even for superconductors with a spatially uniform order parameter. At the same time, one should take into account another significant phenomenon: an inevitable gap amplitude distribution affecting the quasiparticle current, the scatter being either larger or smaller than the instrumental resolution. Lifetime broadening and the gap spread are complementary factors, and it is not a priori known, which of them is more important for a certain tunnel junction.

Multiple-gap features were actually observed long ago even for low-T_c superconductors (see, e.g., [59–61]. Such observations became routine for high-T_c oxides with small coherence lengths [62–64]. The phenomena might be due to at least several reasons: (i) a true multiple-gap (e.g., two-gap) structure of the quasiparticle electron spectrum in the superconducting state [17,65–68] if the Anderson impurity entanglement of different electron wave functions [69] is irrelevant; (ii) a more general kind of an energy gap anisotropy in the momentum ($\boldsymbol{k}$) space [70–73] robust to the impurity influence; (iii) a spatial ($\boldsymbol{r}$ space) inhomogeneity of normal and superconducting electronic properties in the area, which determines the tunnel current of a specific junction [74–76]. Of course, spatial inhomogeneity may be deliberately introduced, e.g., as in the case of the proximity superconductor-normal metal bilayers [77]. Whatever this microscopic background, the simplest possible function $N(E, \Gamma)$, averaged over a gap distribution, can be written down as

$$N(E,\Gamma) = \int_{-\infty}^{+\infty} \left| \mathrm{Re} \frac{E - i\Gamma}{\sqrt{(E - i\Gamma)^2 - \Delta^2}} \right| P(\Delta) d\Delta. \quad (3)$$

Here $P(\Delta)$ is the distribution function of the energy gap values. Since the existence of non-zero Γ and the occurrence of the gap scatter $P(\Delta)$ are mutually independent, they are usually taken into account simultaneously [64]. To be specific, we adopt a random Gaussian distribution function, i.e. $P(\Delta)$ reads

$$P(\Delta) = \frac{1}{\sqrt{2\pi}\delta_0} \exp\left(-\frac{(\Delta - \Delta_0)^2}{2\delta_0^2} \right). \quad (4)$$

Here δ_0 and Δ_0 are a half-width and a mean value of the energy gap distribution, respectively.

3 Results and discussion

Nearly all the conductance curves obtained in our measurements possess zero-bias peaks, as well as modulations and/or fine structures in bias regions. Extra features differ from the gap-related ones. The zero-bias peaks may be a signature of the Josephson effect and/or the constriction weak-link formation. The modulations and/or fine structures are possibly caused by the embedded additional series resistances generated in the main phase of the sample from certain superconducting filaments. The latter are driven into the normal state by the critical current passing through narrow and restricted regions. Alternatively, the fine structures of dI/dV might reflect the excitation of lattice vibrations by the non-stationary (ac) Josephson current, as was suggested, e.g., for high-T_c oxides [78], or the nonlinear self-detection of various harmonics in the Josephson junctions [79]. As for the sub-gap features, the n-particle tunneling [80] might be their origin. Here, to avoid going into those details, although being interesting on their own, we focus on the main representative gap-related structures in dI/dV. It should be noted that normally conducting series resistances, if any, would lead to a redistribution of the applied (measured) bias voltage between those resistances and break junctions themselves. This would result in an overestimation of the deduced energy gaps.

Figure 1 shows representative break-junction tunneling conductances $G(V) = dI/dV$ for $Li_{0.48}(THF)_xHfNCl$. In Figure 1a, dI/dV exhibits highly asymmetric broadened coherent gap peaks with the peak-to-peak separation $V_{p-p} \approx 24$ mV identified by us as $4\Delta(4.2\ K)/e$. The peak intensities are severely suppressed as compared to the calculated SIS-type conductance with the BCS densities of states. Since the peaks should be offset from the origin by $\pm 2\Delta/e$, the gap value is estimated to be $2\Delta \approx 11{-}12$ meV.

In Figure 1a one can also see an additional sub-gap structure and a small zero-bias peak. The broadened and V-shaped conductance background can be attributed to the reactive sample surface because we have obtained more conventional BCS-like conductance features for less-reactive samples. The conductance shown in Figure 1b exhibits slightly smaller Δ than that of Figure 1a, in which small but well-defined coherent peaks are observed with the inner shoulder-like structure.

In Figure 1c another example of the observed dependence $G(V)$ is demonstrated, which is also quite typical for $Li_{0.48}(THF)_xHfNCl$ break junctions. The apparent multiple-gap structure consists of intensive inner peaks at ± 4 mV ($V_{p-p}^{in} \approx 8$ mV) and outer ones of the comparable size near $V \approx \pm 11$ mV ($V_{p-p}^{out} \approx 22$ mV) with a concomitant strong zero-bias peak. The V_{p-p}^{out} values are similar to those of Figures 1a and1b, thus demonstrating reproducibility among the junctions. It is possible to see as well smeared humps at biases $V = \pm 17$ mV larger than the main peak locations at $V = \pm V_{p-p}^{out}/2 \approx \pm 11$ mV, which are discussed later.

Another kind of observed $G(V)$ is shown as an inset in Figure 1c. Here a single-gap structure is found, well fitted by a simple BCS density of states. Therefore, the inner gap-like features seen at $V \approx \pm 4$ mV in Figures 1b and 1c originate most probably from a secondary phase with a small gap, rather than from an SIN junction (N denotes a normal metal) formed instead of the nominal SIS one or from the two-particle tunneling [80].

Tunneling conductances of two different representative $HfNCl_{0.7}$ break junctions are displayed in Figure 2. The high-voltage junction conductance presented in Figure 2a is relatively large, of the order of 0.3 mS, whereas that shown in Figure 2b is as low as $\sim$10 μS. In Figure 2a, clear-cut gap-edge structures at ± 8 mV and a zero-bias

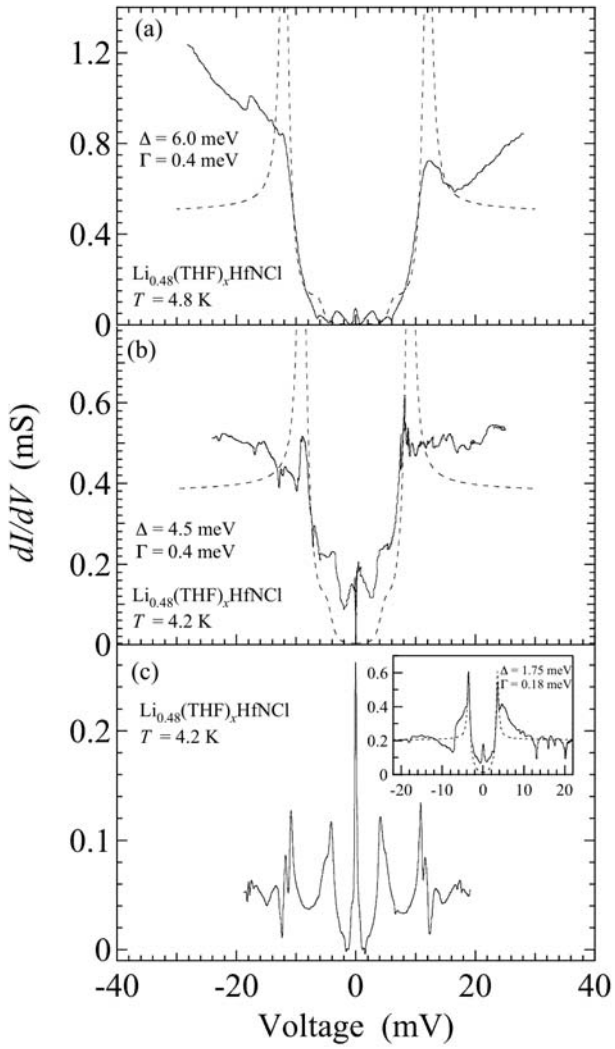

Fig. 1. Voltage, V, dependences of tunneling conductances $G(V) = dI/dV$ for various break-junctions (a, b) and (c) made of $Li_{0.48}(THF)_xHfNCl$ and measured at temperature $T = 4.2$ K. Δ and Γ are the superconducting gap value and the gap broadening, respectively, for realistic superconducting densities of states (see Eq. (2)). The peak-to-peak distance V_{p-p} equals $4\Delta(T)/e$, the break-junctions being of the superconductor-insulator-superconductor (SIS) type. Here e is the elementary charge. Dashed curves are the calculated SIS conductances for the ideal BCS density of states. Inset in (c) shows another $G(V)$ of the same SIS type with the smallest achieved gap value $\Delta \approx 1.75$ meV.

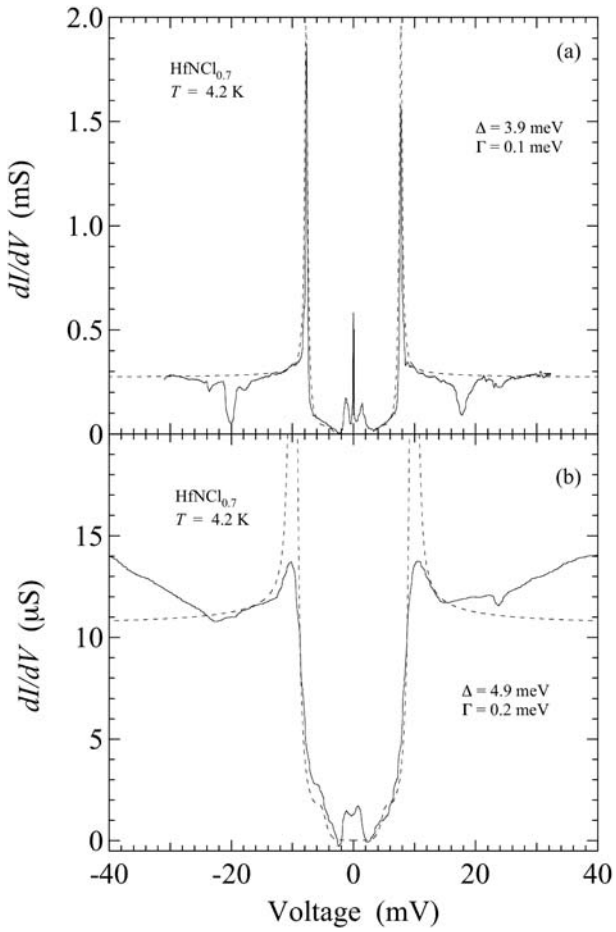

Fig. 2. $G(V)$ for different break junctions made of $HfNCl_{0.7}$ at $T = 4.2$ K. Dashed curves are the calculated BCS conductances for SIS junctions.

Josephson peak are readily seen. A nearly ideal (with a very small damping Γ) BCS density of states with $\Delta \approx 3.9$ meV reproduces the data well including the peak itself. This property is due to the chemically stable sample characteristics. Distinct dip-hump structures outside the gap region might be of intrinsic origin, corresponding to van Hove density-of-states singularities in layered systems [74,75], or be extrinsic, i.e. they might appear due to the current-driven suppression of superconductivity in small weak-link inter-grain contacts [83] or, possibly, at boundaries between segregated phases in the case of phase separation as in cuprates [84,85]. The out-gap structure seems to be too large to be a conventional strong-coupling feature indicating the inelastic boson-assisted electron tunneling [35].

In Figure 2b, the smeared gap-edge peaks at $\pm V_{p-p}/2 \approx \pm 10-11$ mV ($= \pm 2\Delta/e$) are observed with very low leakage and a V-shaped background [34]. A BCS density of states can adequately reproduce the conductance only inside the gap. The additional small sub-gap peaks at approximately $\pm 2-3$ mV in Figures 2a and 2b might be explained by Andreev quasiparticle reflection involving surface proximity effects [35].

To eliminate the V-shaped background, tunneling conductances dI/dV presented in Figures 1a and 1b ($Li_{0.48}(THF)_xHfNCl$ break junctions), and Figure 2b ($HfNCl_{0.7}$ break junction) were divided by $(V)^{1/2}$ and in such a manner normalized quantities were displayed in Figure 3 (a, b, and c, respectively). Such normalization is intended only to get rid of the background, the origin of which is not known. The gap-edge peaks are clearly seen in all panels of Figure 3, and the resulted curves became more similar to $G(V)$ calculated in the framework of the BCS theory than the raw data strongly

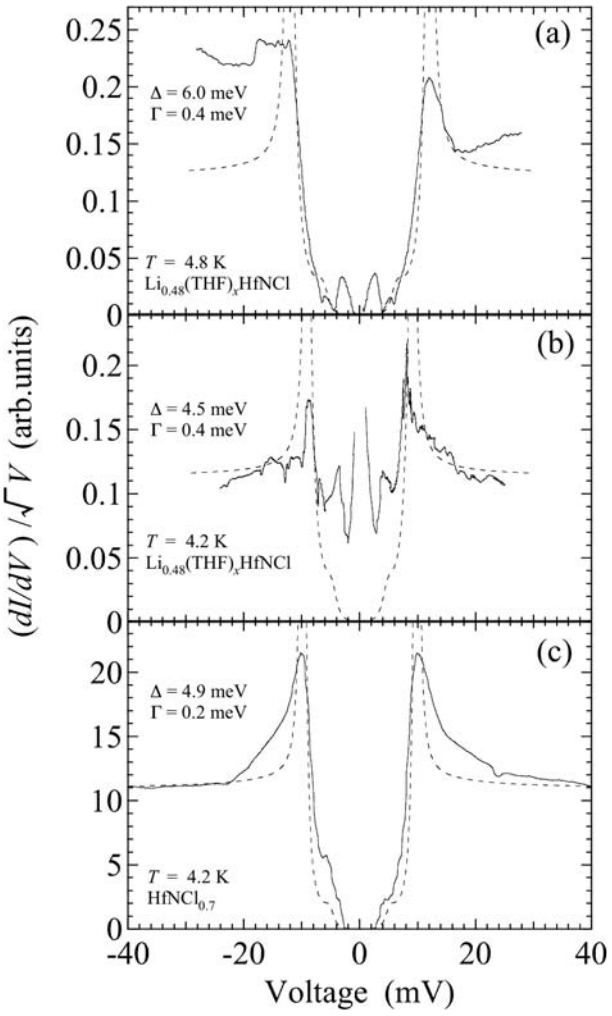

Fig. 3. $G(V)$ divided by $(V)^{1/2}$. Here $G(V)$ correspond to the data presented in Figures 1(a), 1(b) ($Li_{0.48}(THF)_xHfNCl$ break junctions) and 2 (b) ($HfNCl_{0.7}$ break junction), respectively. The dashed curves are the calculated SIS conductances in the framework of the BCS theory.

influenced by the non-superconducting background. The positive-bias gap-edge peak in Figure 3a becomes more conspicuous as compared to that of Figure 1a, whereas the reconstructed dI/dV still exhibits some asymmetry, appropriate to the raw data. In Figure 3b, the normalization by $(V)^{1/2}$ makes the outer coherent peaks more clearly visible and the shoulders at $V \approx \pm 4$ mV are transformed into discernible peaks. In Figure 3c, shoulders appear outside the coherent peaks after the division by $(V)^{1/2}$, and the higher-bias region $|V| > 20$ mV becomes flat. Those shoulders might be a signature of the proximity-induced superconducting gap [35,77]. The introduced $(V)^{1/2}$ dependence of the background presumably reflects scattering of conduction electrons on weakly disordered states in some regions, caused by inhomogeneities left after carrier doping [35].

Figure 4 shows variations of $G(V)$ with T in the gap region for $Li_{0.48}(THF)_xHfNCl$ (a) and $HfNCl_{0.7}$ (b). In both cases, the gap structure is gradually smeared with

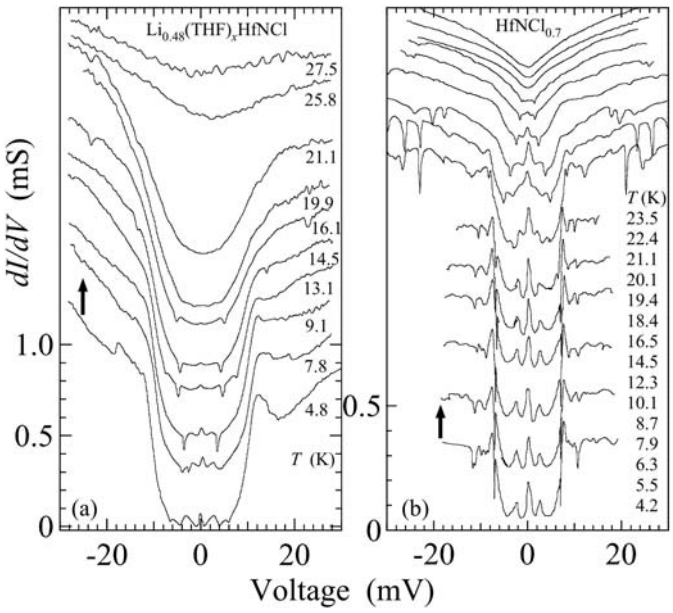

Fig. 4. T variations of $G(V)$ for $Li_{0.48}(THF)_xHfNCl$ (a) and $HfNCl_{0.7}$ (b) break junctions, which were presented in Figures 1a and 2a, respectively.

T to disappear at $T_c = 26$ K (a) and 24 K (b) for $Li_{0.48}(THF)_xHfNCl$ and $HfNCl_{0.7}$, respectively. In particular, one sees from Figure 4b, that $G(V)$ in the neighborhood of the outer gap changes drastically in the range $10 < T < 12$ K but at the same time the inner gap remains almost unchanged, thereby suggesting that either the origin of the features concerned is different or, simply, the outer gap is more affected by spatial scatter. Such an inequality of different gaps has been observed and explained for cuprates, where Cooper and charge-density-wave (CDW) pairings coexist [50,86]. With further increasing of T above 12 K, both gap structures broaden gradually and vanish at the bulk T_c.

Transformation with T of the multiple-gap structure of $G(V)$ for the $Li_{0.48}(THF)_xHfNCl$ break junction, shown above in Figure 1c, is displayed in Figure 5. The gap structures are well defined at low T as shown in Figure 5a. With increasing T, the magnitude of the outer-gap peaks, pronounced at low T, rapidly decreases, so that the peaks evolve into broad humps at approximately 13 K, while the inner peak still remains conspicuous above this T. The zero-bias peak survives up to the bulk T_c. Figure 5b demonstrates vertically expanded spectra to see the detailed structure of $G(V)$ at higher $T > 15$ K. The humps at $V \approx \pm 12$ mV, i.e. outside the inner gap region, disappear at about 21 K, slightly below T_c. The subtle peaks near zero bias, which vanish at $T \approx 13$ K (see Fig. 5a) can be attributed to the gaps, reduced by the proximity effect.

It might be well to point that the apparent V-shapes of $G(V)$ for some junctions does not have to be a consequence of the actual anisotropic nature of the superconducting order parameter leading to an incomplete Fermi surface gapping. Instead, such a behavior might reflect a

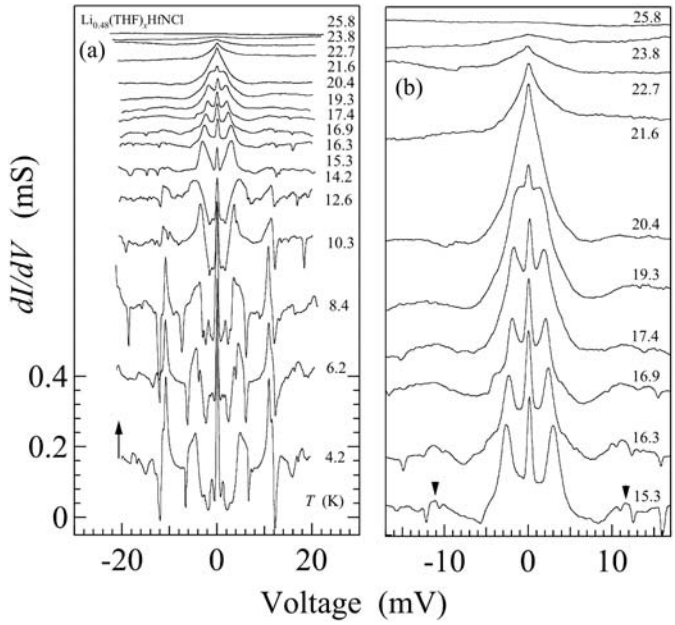

Fig. 5. T variation of the double-peak structure for the sample $Li_{0.48}(THF)_xHfNCl$, presented above in Figure 1c, (a) overall picture up to T_c, (b) enlarged fragment for T near T_c.

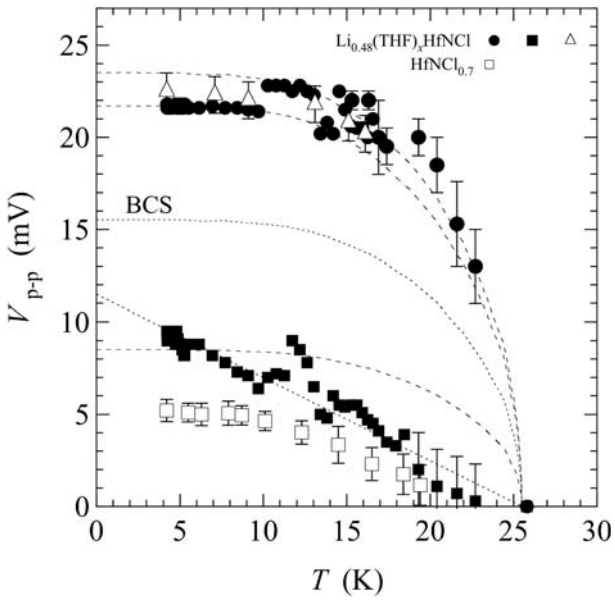

Fig. 6. T-dependences of the peak-to-peak separations V_{p-p} in $G(V)$ for break junctions made of $Li_{0.48}(THF)_xHfNCl$ and $HfNCl_{0.7}$. Closed symbols (• and ■) refer to V_{p-p}^{out} and V_{p-p}^{in}, respectively, correspond to $Li_{0.48}(THF)_xHfNCl$ and are taken from Figure 5. The open symbols (Δ and □) denote peak-to-peak separations found for $Li_{0.48}(THF)_xHfNCl$ (Fig. 4a) and $HfNCl_{0.7}$ (Fig. 4b) break junctions, respectively. Δ corresponds to predominant V_{p-p}, whereas □ describes the inner-gap V_{p-p}^{in}.

contamination of the broken-contact surfaces, which has been shown, e.g., to degrade both the coherent peaks and the overall character of $G(V)$ for $Bi_2Sr_2CaCu_2O_{8+\delta}$ single crystals [87].

In Figure 6, dependences on T of gap values, obtained from the data presented in Figure 5 for $Li_{0.48}(THF)_xHfNCl$ break junctions, are demonstrated. Smearing of the gap features in $G(V)$ at higher T leads to uncertainties of gap values above 20 K, which is shown as large error bars. We note that the gap features with the amplitude $2\Delta(4.2\text{ K}) \approx 11$–$12$ meV ($V_{p-p} \approx 22-24$ mV) for different samples, shown in Figures 4a and 5, exhibit similar T-dependences, which is well expressed by the scaled BCS curve with $T_c = 25.5$ K.

T-dependence of the inner gap for $Li_{0.48}(THF)_xHfNCl$ junctions with $V_{p-p}^{in} \approx 9-10$ mV, shown in Figure 6 and derived from Figure 5, deviates downward from the BCS curve exhibiting almost linear decrease up to the temperatures near bulk T_c. This behavior seems to be a manifestation of the proximity induced gap [35,77] and is similar to that observed in Pb-Sn-PbO-Pb junctions [88] and MgB_2 break junctions with their remarkable multiple-gap structures [89,90]. The latter are usually considered [2] as an intrinsic effect, emerging from the interplay of two superconducting gaps, each originating from a certain electron band [17,65–68]. However, theoretical calculations show that the Fermi surface of $Li_{0.48}(THF)_xHfNCl$ involves a single band [25]. Therefore, possibility of the multiple-band superconductivity in $Li_{0.48}(THF)_xHfNCl$ seems to be ruled out, in particular, as an explanation of the smaller-gap feature. On the contrary, the origin of the proximity effect and the inner gap as its consequence may be local charge-carrier-density inhomogeneities [74–76]. As is readily seen from Figures 1c and 3 (for V_{p-p}^{in}), the small gap is quite reproducible. Therefore, the apparent inner-peak spectra in Figure 1 might be associated with the anisotropy in transport properties [28]. It should be noted that T-dependences of the multiple gap structures displayed in Figures 5 and 6 are similar to those of YNi_2B_2C, where anisotropy of the superconducting gap is considered as their origin [91].

The gap ratio $2\Delta(0)/k_BT_c = 5-5.6$ for $Li_{0.48}(THF)_xHfNCl$ is of the same magnitude as that of the layered superconductor MgB_2 [89,90,92]. As has been already indicated above, this ratio is in fact larger than the weak-coupling BCS value $2\pi/\gamma \approx 3.52$ but much smaller than experimental values for high-T_c cuprates [36] and organic superconductors [37]. For $HfNCl_{0.7}$ samples, the largest attainable gap value $2\Delta(0) \approx 11$ meV is inferred from Figure 2b, whereas $T_c \approx 23.5$ K, so that the ratio $2\Delta(0)/k_BT_c$ becomes 5.4. This is consistent with the results for $Li_{0.48}(THF)_xHfNCl$. The inner-gap small peaks at $V \approx \pm 2.5$ mV ($T = 4.2$ K) taken from Figure 4b and also corresponding to $HfNCl_{0.7}$ break junctions tend to disappear near respective T_c, as is shown in Figure 6 (open squares), although the low-temperature V_{p-p} is half as that for $Li_{0.48}(THF)_xHfNCl$ samples (see Figs. 1b and 1c). If we identify the smaller-gap features for $Li_{0.48}(THF)_xHfNCl$ break junctions with $V_{p-p} \approx 10$ mV with $4\Delta/e$, the ratio $2\Delta(0)/k_BT_c$ becomes 2–2.3. This is substantially smaller than the BCS value, which is consistent with our suggestion that those peaks have the proximity-induced nature.

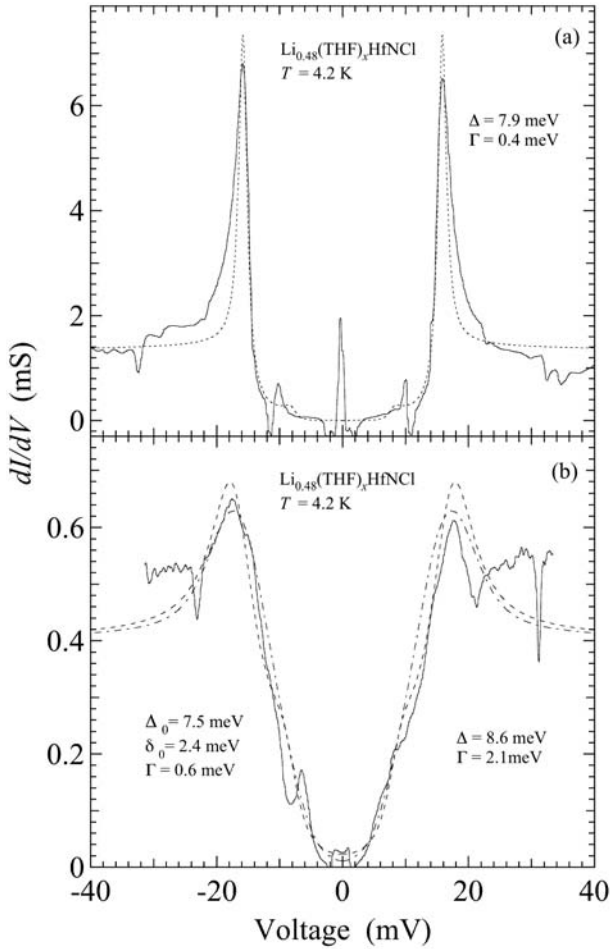

Fig. 7. $G(V)$ with the largest gap values observed in $Li_{0.48}(THF)_xHfNCl$ break junctions. The dashed and dashed-dotted curves describe calculated SIS conductances with the smeared BCS density of states (Eq. (2)) and to that with the Gaussian gap distribution model (Eqs. (3) and (4)), respectively. The spectra (a) and (b) correspond to different break junctions.

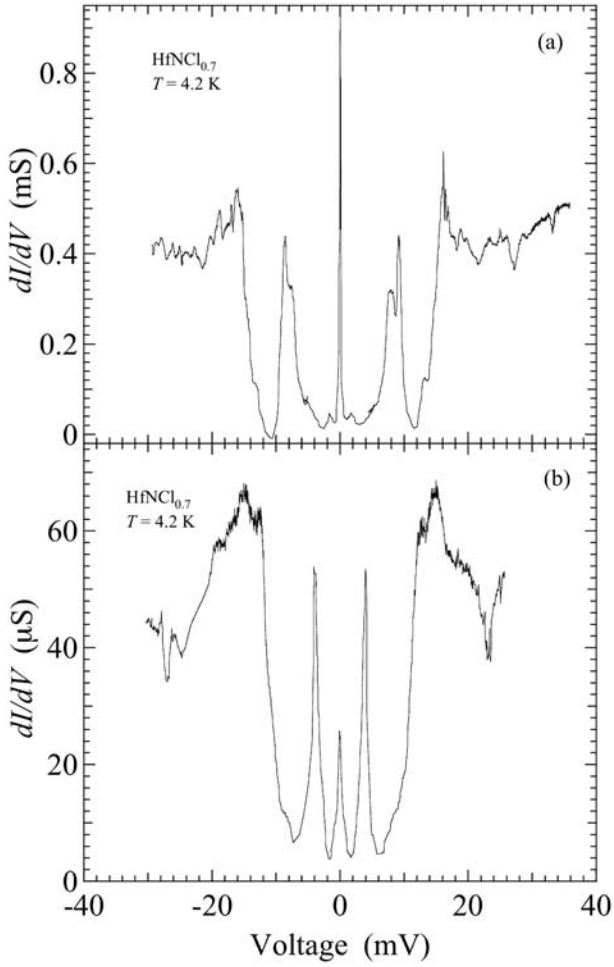

Fig. 8. $G(V)$ with the apparent double-peak structure are presented in (a) and (b) for different $HfNCl_{0.7}$ break junctions.

The widest gap structures in $G(V)$ found by us are shown in Figures 7 and 8 for $Li_{0.48}(THF)_xHfNCl$ and $HfNCl_{0.7}$ break junctions, respectively. Figure 7a exhibits the well-pronounced gap edges around $V \approx \pm 17$ mV and a zero-bias peak, the values corresponding just to the outer peaks in Figure 1c. This $G(V)$ is adequately reproduced by a single-junction SIS current determined by the convolution of BCS density of states (Eq. (1)), indicating that the largest gap-edge energy does not correspond to the intrinsically multiple junctions, as has been found, e.g., for oxide ceramics $BaPb_{1-x}Bi_xO_{3-\delta}$ [93–96] and stacks of tunnel junctions in layered cuprate mesas [97–100]. Conspicuous dip-hump structures are observed at $V \approx \pm 10{-}12$ mV *inside* the gap, the peak locations coinciding with those for the *predominant* coherent gap peaks at $V \approx \pm 11{-}12$ mV for those $Li_{0.48}(THF)_xHfNCl$ junctions, conductances of which are presented in Figure 1.

The gap features of dI/dV measured for another junction and presented Figure 7b are substantially broadened, but their peak positions coincide with locations of fully developed BCS-like peaks in Figure 7a. This gap structure can be reproduced using the Gaussian gap distribution model and/or smeared BCS density of states, the results of fitting calculations exhibited by dashed and dashed-dotted curves. For fittings to be successful, both Γ in equation (2) and δ_0 in equation (3) should be about 0.25 Δ, which is much larger than $\Gamma \approx 0.05\ \Delta$ needed to fit experimental data in Figure 7a. It means that, for certain junctions, dissipation and gap spread becomes essential, probably due to some kind of phase separation and proximity effect.

We observed a large outer gap with a distinct double-gap overall structure in $G(V)$ for $HfNCl_{0.7}$ break junctions, as is shown in Figure 8. The largest gap values are similar to those of $Li_{0.48}(THF)_xHfNCl$ depicted in Figure 7. Such an apparent double-gap structure has been already seen in Figure 1c, although the gap energies are different for different junctions. The outer peak-to-peak distance $V_{p-p}^{out} \approx 32$ mV in Figure 8a is of the same order of magnitude as that in Figure 8b, while the inner-gap parameter $V_{p-p}^{in} \approx 17$ mV in Figure 8a appreciably exceeds $V_{p-p}^{in} = 8{-}10$ mV from Figure 8b. Two values 10 and 17 mV for V_{p-p}^{in} are the same as those given in

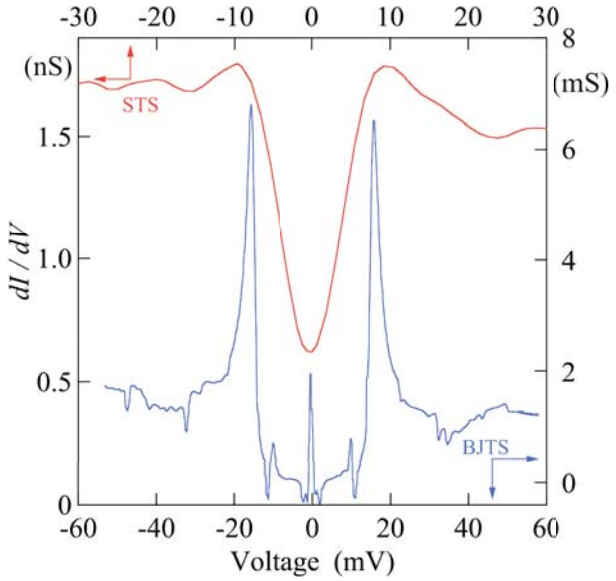

Fig. 9. (Color online) $G(V)$ for SIN junction (STS) between the PtIr tip and $HfNCl_{0.7}$ sample at $T = 5$ K in comparison with that of $Li_{0.48}(THF)_xHfNCl$ SIS break junction (BJTS) at 4 K borrowed from Figure 7a. The bias scale for the SIN junction is twice enlarged to match with the scale for the SIS junction.

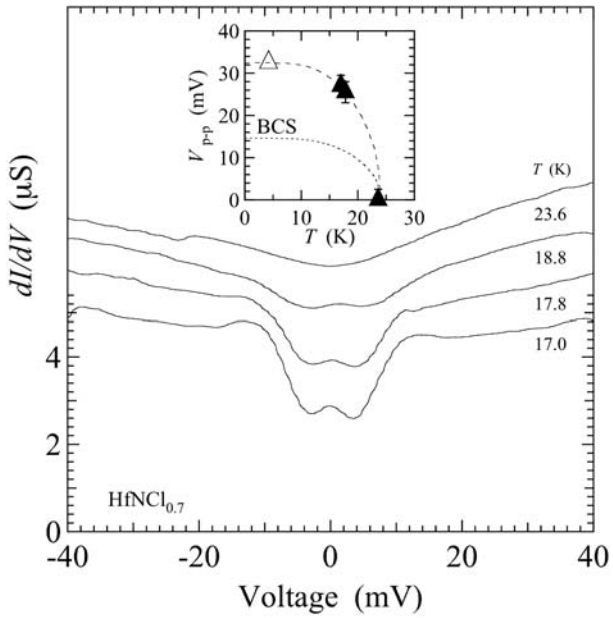

Fig. 10. $G(V)$ for various T for the largest superconducting gap in $HfNCl_{0.7}$. Inset shows the T-dependence of V_{p-p} together with the low-T value V_{p-p}^{out} (open triangle) from Figure 8.

Figures 1 and 2. In particular, the multiple-gap values for $Li_{0.48}(THF)_xHfNCl$ in Figure 1c, $V_{p-p} = 8-10$ mV, 20–22 mV, 34 mV, are quite similar to those for $HfNCl_{0.7}$ in Figures 8a and 8b. Therefore, the spectrum of experimental V_{p-p} involves 8–10 mV, 18–24 mV, and 32–35 mV. To further confirm the existence of the largest $V_{p-p} = 32-35$ mV, we have carried out complementary STS measurements having well-defined vacuum tunneling barrier.

Tunneling (STS) conductance measured at $T = 5$ K in the SIN configuration with a PtIr tip and $HfNCl_{0.7}$ sample is shown in Figure 9. The curve $G(V)$ is asymmetric, i.e., the gap edge for the negative bias (electrons tunnel from the sample to the tip) is more pronounced, and the junction exhibits substantial leakage at zero bias. The gap-edge peaks at $V \approx \pm 10$ mV are discernible, although smeared. The break-junction SIS conductance duplicated from Figure 7a is also displayed in Figure 9 for comparison. Since the compound $Li_{0.48}(THF)_xHfNCl$ is extremely reactive and it is more difficult to measure its tunnel spectra than those of $HfNCl_{0.7}$, STM measurements were done on $HfNCl_{0.7}$. Nevertheless, data for both compounds were displayed in the same Figure 9, because T_c's of $Li_{0.48}(THF)_xHfNCl$ and $HfNCl_{0.7}$ are quite similar (25 K and 24 K) and other electronic properties are basically the same, in spite of the chemical differences. The peak positions of both curves almost coincide after compensatory rescaling between SIN and SIS junctions as is clearly demonstrated in Figure 9. Hence, the extremely large gap features found in break junction measurements are confirmed by STM and can be unambiguously identified with the intrinsic superconducting gaps revealed by quasiparticle tunneling across the SIS junction. Thus, the gap values $2\Delta \approx 16-20$ meV ($V_{p-p} = 32-40$ mV) are inherent to both $Li_{0.48}(THF)_xHfNCl$ and $HfNCl_{0.7}$ compounds.

Figure 10 shows thermal evolution of the break-junction spectrum for another junction, involving $HfNCl_{0.7}$, at high T above 17 K, when the value of $V_{p-p}(T = 17\ \text{K})$ becomes 25 mV. Since this voltage exceeds the representative value of $4\Delta/e = V_{p-p} = 16-20$ mV at 4.2 K, the corresponding junction is probably considered as an example of the systems with the largest gap features appropriate, e.g., to the data presented in Figure 8. The resulting T-dependence of $4\Delta/e = V_{p-p}$ together with its value at 4.2 K, taken from Figure 8, is plotted in the inset of Figure 10. One sees that the observed largest gap value at 4.2 K in Figure 8 is consistent with the extrapolated BCS curve using the gap at 17 K from the main frame of Figure 10 and $T_c = 24$ K. Hence, $G(V)$ displayed in Figure 10 describes the high-T continuation of $G(V)$ with low-T peak-to-peak distance $V_{p-p} = 4\Delta/e \sim 32-35$ mV. From this V_{p-p} (T), the gap ratio is obtained as $2\Delta(0)/k_BT_c = 7.6-8.6$. This value is quite similar to the ratio appropriate to $Li_{0.48}(THF)_xHfNCl$, as stems from Figure 7.

Among the gap energies found for $HfNCl_{0.7}$ in our break-junction studies, the largest gap is typical for STS measurements. The resultant large ratio $2\Delta(0)/k_BT_c$ has been also previously discovered in $ZrNCl_{0.7}$ [34]. Such values are comparable to ratios for high-T_c cuprates [36] or organic superconductors [37], although the origin of the similarity for different classes of materials is not yet clear. We emphasize that the majority of $G(V)$ dependences found here cannot be fitted well by ideal BCS-like SIS characteristics as one would expect for break

junctions, which is not surprising. Indeed, the observed deviations from the textbook appearance might be caused by various reasons, most important of them discussed above. Nevertheless, the peak features are indubitably superconductivity-related ones and the peak-to-peak distances should be identified as multiples of superconducting energy gaps.

The presented break-junction tunneling measurements together with our STS studies indicate that the layered compounds $Li_{0.48}(THF)_xHfNCl$ and $HfNCl_{0.7}$ possesses strikingly large superconducting gaps, which cannot be regarded as a consequence of the conventional strong-coupling superconductivity, involving electron-phonon mechanism of superconductivity. Actually, there are no such conventional superconductors, for which possess $2\Delta(0)/k_BT_c > 5$. The problem of theoretical comprehension of this key dimensionless parameter on the basis of the semi-microscopic Eliashberg gap equations [101,102] has a long history, starting from works of Geilikman et al. [103]. As a result, a number of approximate expressions appeared, containing characteristics of the material phonon spectra [104,105]. Thus, theorists are going beyond the BCS weak-coupling thermodynamic theory of corresponding states, the latter approach leading to *universal* relationships between fundamental quantities, as in the famous van der Waals theory, the first of this sort [106]. For instance, one can employ a frequently used semi-empirical formula for $2\Delta(0)/k_BT_c$ [107]

$$\frac{2\Delta(0)}{k_BT_c} = 3.53\left[1 + 12.5\left(\frac{k_BT_c}{\omega_{\ln}}\right)^2 \ln\left(\frac{\omega_{\ln}}{2k_BT_c}\right)\right], \quad (5)$$

where ω_{ln} is defined as the logarithmic average energy of phonons. The experimental limit 5 implies $\omega_{ln} \approx 12$ meV.

Recent Raman-scattering studies under pressure led to the conclusion that low-energy phonons and the huge electron-phonon coupling constant $\lambda > 3$ constitute a background of superconductivity in MNCl ($ZrNCl_{0.7}$ and $Li_{0.48}(THF)_xHfNCl$) [45]. As stems from our foregoing results, tunnel measurements did not reveal such phonons.

On the other hand, there is some evidence that optical phonons might be the driving force of superconductivity in halides. For instance, Raman scattering studies of Na-intercalated HfNCl showed that the nitrogen vibration modes with energies about 75 meV are broadened by electron doping [108]. The NMR experiments show that the same group of phonons may explain a small isotope effect in $Li_{0.48}(THF)_xHfNCl$ [42]. The neutron scattering measurements by $Li_{1.16}ZrNCl$ samples exhibited phonon softening around 20 meV and 80 meV, mainly corresponding to vibrations of Zr and N ions [109]. Finally, neutron scattering in $Na_{0.3}HfNCl$ showed the increase of intensity around 20–30 meV in the superconducting state [110]. It should be noted that recent first-principle calculations are in good agreement with those experimental results [45].

Theoretical picture of what kind of superconductivity is observed in layered materials studied by us is not at all full and self-consistent. On the one hand, vibrations of light N ions are expected to have large amplitudes, thus implying large anharmonicity and strong electron-phonon interaction [111]. On the other hand, a recent theoretical study of lattice dynamics and electron-phonon interaction in Li_xZrNCl [112] reveal a small coupling constant $\lambda \approx 0.5$. This might indicate, e.g., the necessity to go beyond the Eliashberg theory [101–105]. In particular, the actual pairing might be unconventional, dominated by other gluing bosons and taking into account specific features of layered structures [7–9,113,114].

One should note that the observed values $2\Delta(0)/k_BT_c > 5$ with the large ω_{ln} are similar to those for the largest gap in MgB_2 [89,90,92]. Therefore, the very existence of the layered structures with the honeycomb lattice, involving light-mass ions, might be crucial for superconductivity in both systems.

The smallest gap ratio $2\Delta(0)/k_BT_c \sim 2{-}2.3$ in $Li_{0.48}(THF)_xHfNCl$ and $HfNCl_{0.7}$, as is shown in Figure 5, as well as in $ZrNCl_{0.7}$ [34], indicates that the coexistence of extremely large and small gaps seems to be a common feature for both $HfNCl_{0.7}$ and $ZrNCl_{0.7}$ compounds. Peculiar properties of the electron-phonon interaction, arising from the quasi-two-dimensional character of the material and a strong momentum dependence of the interaction vertex, may also play an important role. In this connection, one can mention a purely electron, e.g., dynamically screened Coulomb mechanism of superconductivity [115–117].

One can notice that the gap value and T_c for $Li_{0.48}(THF)_xHfNCl$ are slightly larger than those of $HfNCl_{0.7}$. This difference could be related to the increase of the basal plane spacing d by the cointercalation. For $Li_{0.48}(THF)_xHfNCl$, THF molecules are cointercalated with Li between Cl layers. The spacing d increases from 0.923 nm for β-HfNCl to 1.87 nm for $Li_{0.48}(THF)_xHfNCl$, while the d value in $HfNCl_{0.7}$ is kept almost unaltered during de-intercalation process [31]. Since the difference in the lattice constant should affect both the phonon dispersion and electron anisotropy, this might cause the change of gaps and T_c. For instance, a slight shift of T_c ($\approx$2 K) has been observed after the co-intercalation of propylene carbonate (PC), when d increased for $Na_{0.28}(PC)_{0.55}HfNCl$ as compared to that for $Na_{0.28}HfNCl$ [118].

The modification of the electron-phonon interaction should affect superconducting properties. So it is no wonder that Raman scattering experiments showed different doping levels result in different linewidths of the A_{1g} optical mode [108]. However, smilar to the case of $ZrNCl_{0.7}$, the detailed measurements demonstrated that high-energy phonons at 77 meV, which are theoretically predicted to be most strongly interacting with conduction electrons, exhibit weaker electron-phonon interaction when T_c increases following the reduction of the doping level [119]. This seems to be in apparent and unexplained contradiction with the assumption that the electron-phonon interaction dominates the Cooper pairing in this compound.

Let us discuss now peculiar large and multiple-gap structures of dI/dV for MNCl compounds. SIS junctions of $HfNCl_{0.7}$ reveal three characteristic gap values, namely, $V_{p-p} = 8{-}10$ mV, 18–24 mV and 32–35 mV, while two peak-to-peak values $V_{p-p} = 7{-}10$ mV and 16–20 mV are observed in $ZrNCl_{0.7}$. Note, that the former two gap values

V_{p-p} = 8−10 mV and 18–24 mV in HfNCl are similar to V_{p-p} = 7−10 mV and 16–20 mV in $ZrNCl_{0.7}$, respectively. The ratio between the largest 32–35 mV and middle 18–24 mV values in $HfNCl_{0.7}$ is roughly similar to that between two gap values in $ZrNCl_{0.7}$. These features could reflect strongly anisotropic electron band structures in investigated layered crystals, as has been shown by band calculations [25,27] as well as noticed in X-ray absorption [30] and μSR [29] experiments.

Magnetization measurements revealed anisotropic upper critical fields in both $HfNCl_{0.7}$ and $ZrNCl_{0.7}$ compounds [28,32] with the anisotropy parameter $\gamma_H = H_{c2//ab}/H_{c2//c} = \xi_c/\xi_{ab} > 1$ (ξ: is the superconducting coherence length), suggesting the anisotropic superconducting gap. Felser et al. [25] predicted that the Fermi surface of electron doped HfNCl is formed by only one band originating from Hf-N hybridized orbital, while for electron doped ZrNCl, three bands are important, originating from Zr–N and Zr–Zr orbitals. Therefore, for $ZrNCl_{0.7}$, a certain fraction of electrons may enter either Zr–Zr band or Zr–N one. For the same doping level $x = 0.3$, carrier density of Hf-N band should be higher than that of Zr–N one. Since the MN (M = Hf or Zr) orbital involves a light-mass element (N), it might be expected that the high-energy mode(s) coupled with doped electrons are responsible for superconductivity. For this reason, it is possible to consider that relatively large doping content in Hf-N band of HfNCl may raise T_c as compared to β-ZrNCl. From the specific heat measurements, the strong-coupling gap ratio $2\Delta(0)/k_BT_c = 4.6-5.2$ is found for $ZrNCl_{0.7}$ [33]. This ratio is similar to our middle-size ratio $2\Delta(0)/k_BT_c = 5-5.6$ for the predominant gap structure, or the average value of the smallest and largest gap ratios taken together (≈2 and ≈8). Specific heat data represent bulk property, while tunneling spectroscopy probe interface local electronic states. Making such an assumption, as above, local and bulk measurements can be reconciled. Actually, similar assumptions work well while describing multiple gap structures in MgB_2 [89,90] and the gap distributions in high-T_c cuprates [120].

4 Conclusion

We have deduced superconducting energy gaps in β-HfNCl ($Li_{0.48}(THF)_x$HfNCl and $HfNCl_{0.7}$) by means of break-junction tunneling spectroscopy. This technique is shown to be effective to elucidate the electronic properties of strongly reactive materials like in the present case. The BCS-like gap structures were obtained, providing evidence for s-wave symmetry of the superconducting gap. For $Li_{0.48}(THF)_x$HfNCl with the highest T_c = 25.5 K, the predominant gap is $2\Delta(4.2\text{ K})$ = 11–12 meV, which corresponds to $2\Delta(0)/k_BT_c = 5-5.6$. In addition, we have observed the largest gap with $2\Delta(4.2\text{ K})$ = 16–18 meV as well as the smallest gap with $2\Delta(4.2\text{ K})$ = 4–5 meV. The highest-gap ratio is estimated to be $2\Delta(0)/k_BT_c \sim 7.5-8.6$, which agrees well with our complementary STM measurements. The results are reproducible and the observed stable features seem to be intrinsic. The latter ratios are 2–3 times larger than the BCS weak-coupling values, whatever the superconducting order-parameter symmetry [121,122], and are quite similar to those for $ZrNCl_{0.7}$, as well as for high-T_c copper-oxide and organic superconductors. Obviously, such a superconductivity phenomenon with the anomalously huge gap is hardly explained even by an extremely strong electron-boson coupling, so that the origin of such large gaps in the framework of the conventional Cooper-pairing concept remains to be elucidated. On the other hand, the forms and temperature dependences of tunnel conductances are in accord with the original BCS picture rather than with the Bose-Einstein-condensate (bipolaron) scenario [123].

This work was supported by a Grant-in-Aid for Scientific Research (Nos. 19540370, 19105006, 19014016) of Japan Society of Promotion of Science. AMG highly appreciates FY2007 fellowship no. S-07042 granted by the Japan Society for the Promotion of Science and the grants given in the framework of the 2009 Visitors Program of the Max Planck Institute for the Physics of Complex Systems (Dresden, Germany).

References

1. J. Nagamatsu, N. Nakagawa, T. Muranaka, Y. Zenitani, J. Akimitsu, Nature **410**, 63 (2001)
2. X.X. Xi, Rep. Prog. Phys. **71**, 116501 (2008)
3. G. Amano, S. Akutagawa, T. Muranaka, Y. Zenitani, J. Akimitsu, J. Phys. Soc. Jpn **73**, 530 (2004)
4. H. Takahashi, K. Igawa, K. Arii, Y. Kamihara, M. Hirano, H. Hosono, Nature **453**, 376 (2008)
5. H. Hosono, J. Phys. Soc. Jpn (Suppl C) **77**, 1 (2008)
6. M. Rotter, M. Tegel, D. Johrendt, Phys. Rev. Lett. **101**, 107006 (2008)
7. M.V. Sadovskii, Uspekhi Fiz. Nauk **178**, 1243 (2008)
8. A.L. Ivanovskii, Uspekhi Fiz. Nauk **178**, 1273 (2008)
9. Yu. A. Izyumov, E.Z. Kurmaev, Uspekhi Fiz. Nauk **178**, 1307 (2008)
10. I.M. Chapnik, Phys. Lett. A **109**, 69 (1985)
11. J.K. Hulm, B.T. Matthias, Science **208**, 881 (1980)
12. M.L. Kulić, Phys. Rep. **338**, 1 (2000)
13. S. Maekawa, T. Tohyama, Rep. Prog. Phys. **64**, 383 (2001)
14. R.S. Markiewicz, J. Phys. Chem. Solids **58**, 1179 (1997)
15. D.J. Scalapino, Phys. Rep. **250**, 329 (1995)
16. A. Bianconi, J. Supercond. **18**, 625 (2005)
17. N. Kristoffel, P. Konsin, T. Örd, Riv. Nuovo Cimento **17**, 1 (1994)
18. I.R. Shein, V.L. Kozhevnikov, A.L. Ivanovskii, Phys. Rev. B **78**, 104519 (2008)
19. M.M. Korshunov, I. Eremin, Phys. Rev. B **78**, 140509 (2008)
20. Yu. G. Naidyuk, I.K. Yanson, O.E. Kvitnitskaya, S. Lee, S. Tajima, Phys. Rev. Lett. **90**, 197001 (2003)
21. T. Takasaki, T. Ekino, R.A. Ribeiro, T. Muranaka, H. Fujii, J. Akimitsu, Physica C **426–431**, 300 (2005)
22. Q. Han, Y. Chen, Z.D. Wang, EPL **82**, 37007 (2008)
23. S. Yamanaka, K. Hotehama, H. Kawaji, Nature **392**, 580 (1998)
24. S. Yamanaka, Annu. Rev. Mater. Sci. **30**, 53 (2000)

25. C. Felser, R. Seshadri, J. Mater. Chem. **9**, 459 (1999)
26. I. Hase, Y. Nishihara, Phys. Rev. B **60**, 1573 (1999)
27. I. Hase, Y. Nishihara, Physica B **281–282**, 788 (2000)
28. H. Tou, Y. Maniwa, K. Ito, S. Yamanaka, Physica C **341–348**, 2139 (2000)
29. T. Ito, Y. Fudamoto, A. Fukaya, I.M. Gat-Malureanu, M.I. Larkin, P.L. Russo, A. Savici, Y.J. Uemura, K. Groves, R. Breslow, K. Hotehama, S. Yamanaka, P. Kyriakou, M. Rovers, G.M. Luke, K.M. Kojima, Phys. Rev. B **69**, 134522 (2004)
30. T. Yokoya, Y. Ishiwata, S. Shin, S. Shamoto, K. Iizawa, T. Kajitani, I. Hase, T. Takahashi, Phys. Rev. B **64**, 153107 (2001)
31. L. Zhu, S. Yamanaka, Chem. Mater. **15**, 1897 (2003)
32. H. Tou, Y.J. Tanaka, M. Sera, Y. Taguchi, T. Sasaki, Y. Iwasa, L. Zhu, S. Yamanaka, Phys. Rev. B **72**, R020501 (2005)
33. Y. Taguchi, M. Hisakabe, Y. Iwasa, Phys. Rev. Lett. **94**, 217002 (2005)
34. T. Takasaki, T. Ekino, H. Fujii, S. Yamanaka, J. Phys. Soc. Jpn **74**, 2586 (2005)
35. E.L. Wolf, *Principles of Electron Tunneling Spectroscopy* (Oxford University Press, New York, 1985)
36. T. Ekino, S. Hashimoto, T. Takasaki, H. Fujii, Phys. Rev. B **64**, 092510 (2001)
37. T. Arai, K. Ichimura, K. Nomura, S. Takasaki, J. Yamada, S. Nakatsuji, H. Anzai, Phys. Rev. B **63**, 104518 (2001)
38. A. Damascelli, Z. Hussain, Z.-X. Shen, Rev. Mod. Phys. **75**, 473 (2003)
39. J.C. Phillips, A. Saxena, A.R. Bishop, Rep. Prog. Phys. **66**, 2111 (2003)
40. J.B. Goodenough, J. Phys.: Condens. Matter **15**, R257 (2003)
41. Ø. Fischer, M. Kugler, I. Maggio-Aprile, C. Berthod, Rev. Mod. Phys. **79**, 353 (2007)
42. H. Tou, Y. Maniwa, S. Yamanaka, Phys. Rev. B **67**, R100509 (2003)
43. Y. Taguchi, T. Kawabata, T. Takano, A. Kitora, K. Kato, M. Takata, Y. Iwasa, Phys. Rev. B **76**, 064508 (2007)
44. W.L. McMillan, Phys. Rev. **167**, 331 (1968)
45. Y. Taguchi, M. Hisakabe, Y. Ohishi, S. Yamanaka, Y. Iwasa, Phys. Rev. B **70**, 104506 (2004)
46. T. Ekino, T. Takabatake, H. Tanaka, H. Fujii, Phys. Rev. Lett. **75**, 4262 (1995)
47. T. Ekino, H. Fujii, M. Kosugi, Y. Zenitani, J. Akimitsu, Phys. Rev. B **53**, 5640 (1996)
48. J.T. Okada, T. Ekino, T. Takasaki, Y. Yokoyama, Y. Watanabe, H. Fujii, S. Nanao, J. Non-Cryst. Solids **312–314**, 513 (2002)
49. J.T. Okada, T. Ekino, Y. Yokoyama, T. Takasaki, Y. Watanabe, S. Nanao, J. Phys. Soc. Jpn **76**, 033707 (2007)
50. T. Ekino, A.M. Gabovich, M.S. Li, M. Pękała, H. Szymczak, A.I. Voitenko, J. Phys.: Condens. Matter **20**, 425218 (2008)
51. R.C. Dynes, V. Narayanamurti, J.P. Garno, Phys. Rev. Lett. **41**, 1509 (1978)
52. W.A. Harrison, Phys. Rev. **123**, 85 (1961)
53. M.H. Cohen, L.M. Falicov, J.C. Phillips, Phys. Rev. Lett. **8**, 316 (1962)
54. D.H. Douglass, Jr., L.M. Falicov, Progr. Low Temp. Phys. **4**, 97 (1964)
55. G.D. Mahan, *Many-Particle Physics* (Kluwer, New York, 2000)
56. J. Bardeen, Phys. Rev. Lett. **6**, 57 (1961)
57. V. Ambegaokar, A. Baratoff, Phys. Rev. Lett. **10**, 486 (1963)
58. I.O. Kulik, I.K. Yanson, *Josephson Effect in Superconducting Tunnel Structures* (Israel Program for Scientific Translation, Jerusalem, 1972)
59. L.Y.L. Shen, N.M. Senozan, N.E. Phillips, Phys. Rev. Lett. **14**, 1025 (1965)
60. L.Y.L. Shen, Phys. Rev. Lett. **29**, 1082 (1972)
61. S.I. Vedeneev, A.I. Golovashkin, G.P. Motulevich, Trudy FIAN SSSR **86**, 140 (1975)
62. J.R. Kirtley, R.M. Feenstra, A.P. Fein, S.I. Raider, W.J. Gallagher, R. Sandstrom, T. Dinger, M.W. Shafer, R. Koch, R. Laibowitz, B Bumble, J. Vac. Sci. Technol. A **6**, 259 (1988)
63. J.R. Kirtley, Int. J. Mod. Phys. B **4**, 201 (1990)
64. B. Barbiellini, Ø. Fischer, M. Peter, Ch. Renner, M. Weger, Physica C **220**, 55 (1994)
65. H. Suhl, B.T. Matthias, L.R. Walker, Phys. Rev. Lett. **3**, 552 (1959)
66. V.A. Moskalenko, Fiz. Metallov I Metalloved **8**, 503 (1959) (in Russian)
67. A.M. Gabovich, E.A. Pashitskii, Ukrain. Fiz. Zhourn. **20**, 1814 (1975) (in Russian)
68. A. Bussmann-Holder, L. Genzel, A. Simon, A.R. Bishop, Z. Phys. B **92**, 149 (1993)
69. P.W. Anderson, J. Phys. Chem. Sol. **11**, 26 (1959)
70. V.L. Pokrovsky, M.S. Ryvkin, Zh. Eksp. Teor. Fiz. **43**, 92 (1962)
71. D.W. Youngner, R.A. Klemm, Phys. Rev. B **21**, 3890 (1980)
72. S.V. Pokrovsky, V.L. Pokrovsky, Phys. Rev. B **54**, 13275 (1996)
73. M.B. Walker, Phys. Rev. B **64**, 134515 (2001)
74. A.M. Gabovich, A.I. Voitenko, Phys. Rev. B **60**, 7465 (1999)
75. A.M. Gabovich, Mai Suan Li, M. Pękała, H. Szymczak, A.I. Voitenko, Physica C **405**, 187 (2004)
76. T. Ekino, A.M. Gabovich, Mai Suan Li, T. Takasaki, A.I. Voitenko, J. Akimitsu, H. Fujii, T. Muranaka, M. Pękała, H. Szymczak, Physica C **426–431**, 230 (2005)
77. Z. Long, M.D. Stewart, Jr., T. Kouh, J.M. Valles, Jr., Phys. Rev. Lett. **93**, 257001 (2004)
78. Ya. G. Ponomarev, E.B. Tsokur, M.V. Sudakova, S.N. Tchesnokov, M.E. Shabalin, M.A. Lorenz, M.A. Hein, G. Müller, H. Piel, B.A. Aminov, Solid State Communs. **111**, 513 (1999)
79. N.R. Werthamer, Phys. Rev. **147**, 255 (1966)
80. J.R. Schrieffer, J.W. Wilkins, Phys. Rev. Lett. **10**, 17 (1963)
81. M. Tachiki, S. Takahashi, F. Steglich, H. Adrian, Zeit. Physik **80**, 161 (1990)
82. T.G. Miller, M. McElfresh, R. Reifenberger, Phys. Rev. B **48**, 7499 (1993)
83. K.K. Likharev, Rev. Mod. Phys. **51**, 101 (1979)
84. E.L. Nagaev, Uspekhi Fiz. Nauk **165**, 529 (1995)
85. E.V.L. de Mello, E.S. Caixeiro, Phys. Rev. B **70**, 224517 (2004)
86. T. Ekino, A.M. Gabovich, Mai Suan Li, M. Pękała, H. Szymczak, A.I. Voitenko, Phys. Rev. B **76**, 180503 (2007)
87. Ch. Renner, Ø. Fischer, Phys. Rev. B **51**, 9208 (1995)

88. A. Gilabert, J.P. Romagnan, E. Guyon, Solid State Commun. **9**, 1295 (1971)
89. T. Ekino, T. Takasaki, T. Muranaka, J. Akimitsu, H. Fujii, Phys. Rev. B **67**, 094504 (2003)
90. T. Takasaki, T. Ekino, T. Muranaka, T. Ichikawa, H. Fujii, J. Akimitsu, J. Phys. Soc. Jpn **73**, 1902 (2004)
91. P. Raychaudhuri, D. Jaiswal-Nagar, G. Sheet, S. Rarnakrishnan, H. Takeya, Phys. Rev. Lett. **93**, 156802 (2004)
92. T. Ekino, T. Takasaki, H. Fujii, S. Yamanaka, Physica C **388–389**, 573 (2003)
93. N.A. Belous, A.M. Gabovich, I.V. Lezhnenko, D.P. Moiseev, V.M. Postnikov, S.K. Uvarova, Phys. Lett. A **92**, 455 (1982)
94. N.A. Belous, A.E. Chernyakhovskii, A.M. Gabovich, D.P. Moiseev, V.M. Postnikov, J. Phys. C: Solid State Phys. **21**, L153 (1988)
95. Y. Enomoto, M. Suzuki, T. Murakami, T. Inukai, T. Inamura, Jpn. J. Appl. Phys. **20**, L661 (1981)
96. M. Suzuki, Y. Enomoto, T. Murakami, J. Appl. Phys. **56**, 2083 (1984)
97. V.M. Krasnov, A. Yurgens, D. Winkler, P. Delsing, T. Claeson, Phys. Rev. Lett. **84**, 5860 (2000)
98. A.A. Yurgens, Supercond. Sci. Technol. **13**, R85 (2000)
99. A. Yurgens, M. Torstensson, L.X. You, T. Bauch, D. Winkler, I. Kakeya, K. Kadowaki, Physica C **468**, 674 (2008)
100. M. Suzuki, T. Watanabe, Phys. Rev. Lett. **85**, 4787 (2000)
101. G.M. Eliashberg, Zh. Eksp. Teor. Fiz. **38**, 966 (1960)
102. G.M. Eliashberg, Zh. Eksp. Teor. Fiz. **39**, 1437 (1960)
103. B.T. Geilikman, V.Z. Kresin, N.F. Masharov, J. Low Temp. Phys. **18**, 241 (1975)
104. P.B. Allen, B. Mitrović, Solid State Phys. **37**, 1 (1982)
105. J.P. Carbotte, Rev. Mod. Phys. **62**, 1027 (1990)
106. D. Kondepudi, I. Prigogine, *Modern Thermodynamics. From Heat Engines to Dissipative Structures* (John Wiley and Sons, Chichister, 1999)
107. F. Marsiglio, J.P. Carbotte, Phys. Rev. B **33**, 6141 (1986)
108. A. Cros, A. Cantarero, D. Beltran-Porter, J. Oro-Sole, A. Fuertes, Phys. Rev. B **67**, 104502 (2003)
109. P. Adelmann, B. Renker, H. Schober, M. Braden, F. Fernandez-Diaz, J. Low. Temp. Phys. **117**, 449 (1999)
110. S. Shamoto, K. Iizawa, T. Koiwasaki, M. Yasukawa, S. Yamanaka, O. Petrenko, S.M. Bennington, H. Yoshida, K. Ohoyama, Y. Yamaguchi, Y. Ono, Y. Miyazaki, T. Kjitani, Physica C **341–348**, 747 (2000)
111. N. Tsuda, Private communications
112. R. Heid, K.–P. Bohnen, Phys. Rev. B **72**, 134527 (2005)
113. K. Kuroki, S. Onari, R. Arita, H. Usui, Y. Tanaka, H. Kontani, H. Aoki, Phys. Rev. Lett. **101**, 087004 (2008)
114. K. Kuroki, Sci. Technol. Adv. Mater. **9**, 044202 (2008)
115. E.A. Pashitskii, Yu. A Romanov, Ukrain. Fiz. Zhourn. **15**, 1594 (1970) (in Russian)
116. Y. Takada, J. Phys. Soc. Jpn **45**, 786 (1978)
117. A. Bill, H. Morawitz, V.Z. Kresin, Phys. Rev. B **66**, R100501 (2002)
118. S. Yamanaka, K. Hotehama, T. Koiwasaki, H. Kawaji, H. Fukuoka, S. Shamoto, T. Kawajiri, Physica C **341–348**, 699 (2000)
119. A. Kitora, Y. Taguchi, Y. Iwasa, J. Phys. Soc. Jpn **76**, 023706 (2007)
120. K.M. Lang, V. Madhavan, J.E. Hoffman, E.W. Hudson, H. Eisaki, S. Uchida, J.C. Davis, Nature **415**, 412 (2002)
121. A.A. Abrikosov, *Modern Thermodynamics. Fundamentals of the Theory of Metals* (North-Holland, Amsterdam, 1987)
122. H. Won, K. Maki, Phys. Rev. B **49**, 1397 (1994)
123. A.S. Alexandrov, J. Phys: Condensed Matter **19**, 125216 (2007)